^{18}F-Fluoroestradiol Tumor Uptake Is Heterogeneous and Influenced by Site of Metastasis in Breast Cancer Patients

Hilde H. Nienhuis[1], Michel van Kruchten[1], Sjoerd G. Elias[2], Andor W.J.M. Glaudemans[3], Erik F.J. de Vries[3], Alfons H.H. Bongaerts[†3], Carolien P. Schröder[1], Elisabeth G.E. de Vries[1], and Geke A.P. Hospers[1]

[1]Department of Medical Oncology, University of Groningen, University Medical Center Groningen, Groningen, The Netherlands; [2]Department of Epidemiology, Julius Center for Health Sciences and Primary Care, University Medical Center Utrecht, Utrecht, The Netherlands; and [3]Department of Nuclear Medicine and Molecular Imaging, University of Groningen, University Medical Center Groningen, Groningen, The Netherlands

See an invited perspective on this article on page 1210.

Heterogeneity of estrogen receptor (ER) expression in breast cancer is recognized. However, knowledge about varying expression across metastases and surrounding normal tissue in patients is scarce. We therefore analyzed 16α-^{18}F-fluoro-17β-estradiol (^{18}F-FES) PET to assess ER expression heterogeneity. **Methods:** ^{18}F-FES PET on accredited PET/CT camera systems performed in patients with ER-positive metastatic breast cancer November 2009–December 2014 was analyzed. Lesions with an SUV_{max} 1.5 or more were considered ER-positive, but liver lesions were excluded given high background liver signal. CT lesions with a diameter 10 mm or more were included. We used multilevel linear-mixed models to evaluate determinants of ^{18}F-FES uptake. Cluster analysis was performed with different imaging features per patient as input variables. **Results:** In 91 patients, 1,617 metastases in bone (78%), lymph node (15%), lung (4%), or liver (2%) were identified by CT (11.2%), PET (56.6%), or both (32.2%). Median tumor uptake varied greatly between patients (SUV_{max}, 0.54–14.21). ^{18}F-FES uptake in bone metastases was higher than in lymph node and lung metastases (geometric mean SUV_{max}, 2.61 [95% confidence interval (CI), 2.31–2.94] vs. 2.29 [95% CI, 2.00–2.61; $P < 0.001$] vs. 2.23 [95% CI, 1.88–2.61; $P = 0.021$]), respectively. Cluster analysis identified 3 subgroups of patients characterized by particular metastatic sites and ^{18}F-FES PET/CT features. SUV_{max} in surrounding normal tissue, highest in the bones, varied per patient (range, 0.7–3.3). **Conclusion:** ^{18}F-FES uptake is heterogeneous in tumor and normal tissue and influenced by anatomic site. Different patterns can be distinguished, possibly identifying biologically relevant ER-positive metastatic breast cancer patient subgroups.

Key Words: breast cancer; estrogen receptor; ^{18}F-fluoroestradiol PET; tumor heterogeneity; tumor microenvironment

J Nucl Med 2018; 59:1212–1218
DOI: 10.2967/jnumed.117.198846

Breast cancer is the most common cause of cancer death among women (*1*). Data are accumulating that both inter- and intralesional differences occur in breast cancer patients (*2*). This heterogeneity is thought to be caused by clonal selection due to intrinsic cellular factors such as genetic mutations and extrinsic factors as paracrine signaling (*3*). This implies that tumor characteristics can be different within a tumor lesion as well as between metastases within the same patient (*4*).

Currently, the most important molecular characteristic of breast cancer is the estrogen receptor (ER). Targeting the ER by hormonal therapy is one of the pillars of breast cancer treatment in the adjuvant as well as metastatic setting (*5*). Tumor response to this treatment is mainly dependent on the ER expression by the tumor cells, which is the case in approximately 75% of all breast cancers (*6*).

However, discrepant ER expression between primary tumor and metastases is on average present in about 20% of the breast cancer patients (*7,8*). Currently, limited knowledge is available about differences in ER expression between metastatic sites. Increasing our understanding of ER heterogeneity could aid in providing precision medicine regarding endocrine therapy of breast cancer patients (*4*).

Generally, ER status is determined by immunohistochemistry on biopsy material of the primary tumor or a metastasis. Whole-body visualization and quantification of ER of all lesions within 1 patient can be performed by PET imaging with 16α-^{18}F-fluoro-17β-estradiol (^{18}F-FES) as a tracer. Uptake of the tracer in tumor lesions correlates well with ER expression in the tumor lesions measured with immunohistochemistry (*9*). Therefore, ^{18}F-FES PET provides whole-body information regarding ER status and enables quantification of ER expression in the primary tumor and metastases in patients (*10*). In addition, this method allows visualization and quantification of ER expression in normal tissue surrounding metastases.

In this study, we aimed to analyze heterogeneity of metastatic breast cancer and its surrounding normal tissue based on ^{18}F-FES uptake between and within ER-positive metastatic breast cancer patients, taking into account the site of metastases. Furthermore, we explored the presence of distinct patterns of ER-positive metastatic breast cancer defined by ^{18}F-FES PET/CT imaging results.

MATERIALS AND METHODS

Patient Population

^{18}F-FES PET scans were obtained in patients with newly diagnosed metastatic breast cancer as well as patients receiving prior hormonal of chemotherapeutic treatment for metastatic disease. Scans between

Received Jul. 27, 2017; revision accepted Mar. 21, 2018.
For correspondence or reprints contact: Geke A.P. Hospers, Department of Medical Oncology, University Medical Center Groningen, Hanzeplein 1, P.O. Box 30.001, 9700 RB Groningen, The Netherlands.
E-mail: g.a.p.hospers@umcg.nl
[†]Deceased.
Published online Mar. 30, 2018.

November 2009 and December 2014 were reanalyzed. All patients had biopsy-proven ER-positive breast cancer (primary and/or metastatic) based on immunohistochemistry. ^{18}F-FES PET scans of all consecutive patients, within this time frame in the University Medical Center Groningen, were analyzed for inclusion.

Excluded were scans that were not obtained using a dedicated PET/CT camera, scans obtained in patients diagnosed with nonbreast cancer metastases, and scans obtained in ongoing ^{18}F-FES PET studies (ClinicalTrials.gov identifier NCT01957332 and NCT01988324) (Supplemental Fig. 1; supplemental materials are available at http://jnm.snmjournals.org). Included in this analysis were patients who underwent scans as routine care or baseline ^{18}F-FES PET scans when enrolled in completed ^{18}F-FES PET studies (*11,12*). Conforming to Dutch Law and retrospective study design, no informed consent of the patients was needed.

^{18}F-FES PET/CT

^{18}F-FES PET scans were obtained as described earlier (*13*). ^{18}F-FES was administered intravenously in a dose of approximately 200 MBq. Whole-body ^{18}F-FES PET was performed 60 min after tracer injection, using European Association of Nuclear Medicine Research Ltd.–accredited PET/CT camera systems (Siemens CTI), high definition and time-of-flight, and 2-mm spatial resolution. Emission scans were acquired for 3 min per bed position, and a low-dose CT-scan was obtained for attenuation correction. In some patients a contrast-enhanced CT was acquired as well. All scans and quantifications were performed according to the guidelines for tumor ^{18}F-FDG PET of the European Association of Nuclear Medicine (*14*). Scans were reconstructed with a Gaussian filter of 5 mm in full width at half maximum, using image matrixes of 256 × 256 mm, and iterative reconstruction methods were used with 3 iterations and 24 subsets.

Analysis of Imaging Results

^{18}F-FES PET and low-dose or contrast-enhanced CT scans were evaluated for the presence of lesions. For 54 patients (59.3%), a contrast-enhanced CT scan was available. Lesions detected by ^{18}F-FES-PET were recorded, and ^{18}F-FES uptake was quantified. Congruent with our previous ^{18}F-FES PET studies, the SUV_{max} was used to quantify ER expression. Lesions with an SUV_{max} of 1.5 or more were considered ^{18}F-FES–positive (*13,14*).

Because of this high physiologic ^{18}F-FES liver uptake (*15*), liver lesions were excluded from quantitative analyses. Background ^{18}F-FES uptake in various healthy tissue types, including fat, lung, liver, muscle and bone, was quantified in all individual patients. Various bones were considered (skull, cervical spine, thoracic spine, lumbar spine, and femur). Background measures were not performed if interference by metastatic lesions was plausible.

CT data were used to allocate PET-positive lesions to an anatomic substrate, to identify ^{18}F-FES PET–negative lesions, and for the detection of liver lesions. Low-dose CT scans were evaluated by an experienced radiologist for presence of metastases. Contrast-enhanced CT scans performed within 6 wk of ^{18}F-FES PET scan were also eligible for analysis. CT results were compared with findings on ^{18}F-FES PET. Lesions present on CT, but negative on ^{18}F-FES PET, were quantified on ^{18}F-FES PET by obtaining the SUV_{max} of a volume of interest drawn on fused PET/CT images. Only CT lesions with a width of minimally 10 mm were included for identification of ^{18}F-FES PET–negative lesions, because lesions of 10 mm or more may be false-negative on ^{18}F-FES PET due to resolution limitations.

Statistical Analysis

First, we evaluated the frequency of metastases visible on CT and/or ^{18}F-FES PET according to site, and within and between patients. Site-to-site variability in ^{18}F-FES uptake was expressed as the coefficient of variation (SD/mean). Liver lesions were excluded from quantitative analyses.

TABLE 1
Patient Characteristics

Characteristic	All patients, n = 91
Median age (y)	61 (range, 33–83)
Sex (*n*)	
Female	90 (99%)
Male	1 (1%)
Median time from primary tumor to metastasis (y)	5 (range, 0–22)
Primary tumor immunohistochemistry receptor status	
ER (*n*)	
Positive	85 (97%)
Negative*	3 (3%)
Unknown*	3
PR (*n*)	
Positive	64 (83%)
Negative	13 (17%)
Unknown	14
Human epidermal growth factor receptor 2 (*n*)	
Positive	11 (18%)
Negative	50 (82%)
Unknown	30
Second primary breast malignancy	17 (19%)
ER antagonist use before ^{18}F-FES PET (*n*)	
Median stop duration (wk)	5.2 (range, 3–11)
Receptor discordance primary tumor and metastasis	
ER (*n*)/total patient with known receptor status	
Concordant	29/35 (83%)
Positive to negative	5/35 (14%)
Negative to positive	1/35 (3%)
PR (*n*)	
Concordant	23/29 (79%)
Positive to negative	5/29 (17%)
Negative to positive	1/29 (3%)
Human epidermal growth factor receptor 2	
Concordant	17/18 (94%)
Positive to negative	1/18 (6%)
Negative to positive	0/18 (0%)

*Metastatic lesion or secondary primary breast cancer ER-positive on immunohistochemistry.

To assess the relation between site and ^{18}F-FES uptake in unaffected tissue and metastases, we used multilevel linear mixed models, taking within-patient clustering into account as random intercept. ^{18}F-FES uptake was first evaluated continuously following natural

TABLE 2
Sites of Metastases

Site	All metastases, n = 1,617
Brain (*n*)	2 (0.1%)
Breast (*n*)	12 (1%)
Lung (*n*)	60 (4%)
Liver (*n*)	29 (2%)
Bone (*n*)	1,257 (78%)
Skull	78 (5%)
Cervical spine	78 (5%)
Thoracic spine	282 (17%)
Lumbar spine	158 (10%)
Pelvis	242 (15%)
Sternum	47 (3%)
Clavicle/humerus	107 (7%)
Rib	210 (13%)
Femur	55 (3%)
Lymph node (*n*)	243 (15%)
Cervical/supraclavicular	59 (4%)
Mediastinal	125 (8%)
Axilla	46 (3%)
Abdomen/pelvis	13 (1%)
Other (*n*)	14 (1%)

log transformation to obtain approximate normal distributions (yielding geometric mean differences upon backtransformation). We also evaluated metastatic ^{18}F-FES uptake binary considering an $SUV_{max} \geq 1.5$ as ^{18}F-FES PET–positive (yielding absolute differences in percentage ^{18}F-FES PET–positive metastases). We similarly studied the influence of ER-antagonist use on ^{18}F-FES uptake, and mutually corrected the effects of ER-antagonist use and metastasis site by including both variables simultaneously in the models. *P* values and 95% CIs for these linear mixed model analyses were obtained by 2,000-fold bootstrap resampling, and a nominal α of <0.05 was considered significant.

Finally, we explored whether metastatic breast cancer patients with ER-positive disease can be clustered into distinct groups based on ^{18}F-FES PET/CT imaging results. For this we used agglomerative hierarchical Ward clustering with Spearman's rho as distance measure, based on 13 patient-based imaging features: the number of metastases visible on ^{18}F-FES PET and/or CT, overall and per site (bone, brain, breast, liver, lung, and lymph nodes); the overall number and percentage of metastases visible on CT respectively being ^{18}F-FES PET–positive; and the mean and standard deviation of ^{18}F-FES SUV_{max}, for all nonliver metastases. We determined the appropriate number of clusters based on a majority vote using 30 indices. We then tested for differences between clusters in the distribution of above imaging features using the Kruskall–Wallis rank-sum test and report those imaging features that were statistically significant following Bonferroni correction (i.e., with a critical α of 0.05/13 = 0.0038).

Statistical analyses were performed in R (R Foundation; 3.2.1 for Mac OS, particularly using the function hclust from the package stats, NbClust from the package NbClust, and lmer from the package lme4) (*16*). All reported *P* values are 2-sided.

RESULTS

Patients

In total, 91 patients were included for analyses. Six of them were premenopausal (flow chart diagram, Supplemental Fig. 1). Twenty-eight patients discontinued ER antagonists (22 tamoxifen, 6 fulvestrant) use a median 5.2 wk before the ^{18}F-FES PET scan.

Patient and tumor characteristics are listed in Table 1 and Supplemental Table 1. The mean time between ^{18}F-FES PET scanning and biopsy of primary tumor and metastasis was 9 y (range, 0–29 y) and 3 y (range, 0–16 y), respectively.

Distribution of Metastases by Anatomic Site

In total, 1,617 lesions were identified in 91 patients. These lesions were identified on either CT (n = 181; 11.2%), on ^{18}F-FES PET (n = 915; 56.6%), or both (n = 521; 32.2%). Lesions were present in bone (78%), lymph nodes (15%), lung (4%), liver (2%), breast (1%), brain (0.1%), and other sites (1%). Distribution of metastases by their location is presented in Table 2. The median number of lesions per patient was 9 (range, 1–110). The ^{18}F-FES uptake of all metastases in the 91 individual patients is depicted in Figure 1.

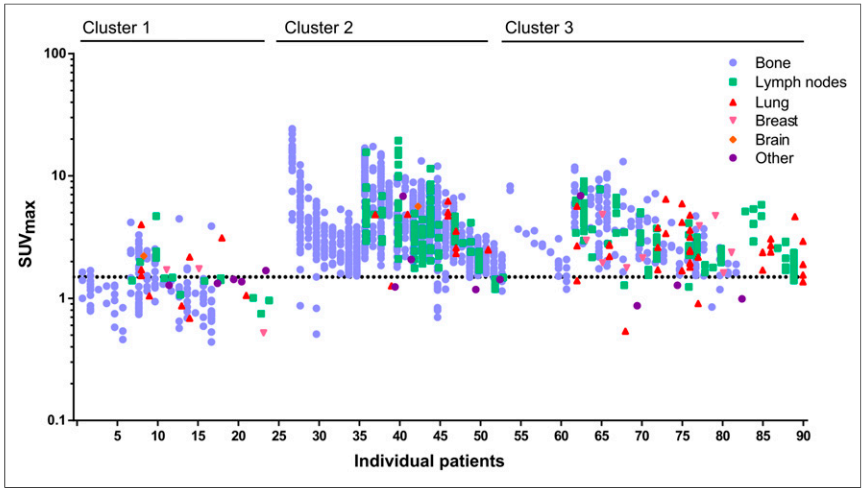

FIGURE 1. Distribution of metastases per patient. Distribution and ^{18}F-FES uptake of all metastases (n = 1,617) in 91 individual patients. Bone (blue), lymph node (green), lung (red), breast (pink), brain (orange), and other (purple) lesions are presented. Patients are categorized on the basis of subgroups derived from the cluster analysis.

Inter- and Intrapatient Heterogeneity of ^{18}F-FES Uptake by Metastases

Median SUV_{max} per patient varied between 0.54 and 14.21. The SUV_{max} of ^{18}F-FES–positive lesions varied up to 11-fold within individual patients (range per patient, 1.8–19.4). Most patients had one or more ^{18}F-FES–positive lesions (78 patients; 86%); in 45 patients (49%), all lesions were ^{18}F-FES–positive. In 44 patients (48%), one or more negative lesions were identified; in 11 patients (12%) only ^{18}F-FES–negative lesions were detected. Thus, in 33 patients (36%) ^{18}F-FES–positive as well as –negative lesions were identified. Two patients had only liver metastases (2%). Univariate analysis showed a trend toward lower SUV_{max} for patients with human epidermal growth factor receptor 2–positive primary disease (geometric mean SUV_{max}, 1.68 [1.10–2.52]) compared with human

TABLE 3
Three Distinct ER-Positive Metastatic Breast Cancer Subgroups as Identified by Agglomerative Hierarchical Cluster Analysis of ^{18}F-FES PET/CT

Imaging features	Group 1 (n = 26)	Group 2 (n = 27)	Group 3 (n = 38)	P
Number of metastases, overall	3.5 (2.0–10.8)	33.0 (22.0–55.0)	5.5 (3.0–10.8)	7.45E−11
Number of metastases, bone	2.0 (0.0–7.8)	26.0 (19.0–47.5)	2.0 (1.0–5.0)	1.35E−11
Geometric mean ^{18}F-FES SUV_{max}	1.1 (1.0–1.4)	3.4 (2.5–4.7)	2.7 (2.3–3.6)	7.29E−12
Percentage metastases visible on CT per patient	100.0 (94.6–100.0)	40.0 (28.2–59.5)	55.0 (31.8–96.9)	9.96E−09
Percentage metastases positive on ^{18}F-FES PET	3.6 (0.0–31.2)	100.0 (90.9–100.0)	100.0 (91.0–100.0)	6.27E−14
Number of metastases visible on CT	3.0 (2.0–10.0)	14.0 (5.5–24.5)	2.5 (1.0–5.0)	9.36E−07
Number of metastases positive on ^{18}F-FES PET	0.5 (0.0–1.0)	28.0 (20.0–54.5)	5.5 (2.2–9.0)	6.99E−14

Imaging features were first assessed on a patient level and then summarized per group as medians, with interquartile ranges in parentheses; P values are based on Kruskal–Wallis rank sum tests.

epidermal growth factor receptor 2–negative primary disease (geometric mean SUV_{max}, 2.57 [2.15–3.06]) (P = 0.058). The coefficient of variation was high for all metastatic sites, namely 61% for lung metastases, 47% for lymph node metastases, and 57% for bone metastases.

With agglomerative hierarchical clustering of imaging features, 3 clusters of patients were identified (Table 3; Supplemental Fig. 2). The clusters identified with this unbiased approach correspond with distinct patterns characterized by particular metastatic sites and ^{18}F-FES uptake. As shown in Table 3, patients in group 1 (n = 26, 29%) have the lowest number of metastases, which are almost always visible on CT but are seldom ^{18}F-FES PET–positive. On the other hand, metastases from patients in group 2 (n = 27, 30%) and group 3 (n = 38, 42%) are nearly always ^{18}F-FES PET–positive and are visible on CT in about 50%. The predominant difference between group 2 and 3 is the number of metastases, with a median of 33 metastases per patient in group 2 (particularly bone metastases). The percentage of patients using ER antagonists was different between the clusters (group 1, 46%; group 2, 11%; and group 3, 24% ([P = 0.013]), but ER antagonist use did not contribute to the cluster formation.

Pattern of Varying ^{18}F-FES Uptake by Metastases, per Site

^{18}F-FES uptake in metastases differed per site in the body. Geometric mean SUV_{max} of bone metastases was 2.61 (95% CI, 2.31–2.94) compared with 2.29 (95% CI, 2.00–2.61) for lymph nodes and 2.23 (95% CI, 1.88–2.64) for lung metastases. Lymph node metastases showed on average 12.4% (95% CI, 6.2–18.3; P < 0.001) and lung metastases 14.7% (2.5–25.5; P = 0.021) lower SUV_{max} than bone metastases. These differences remained present after correction for recent ER antagonist use (respectively, 12.4% and 14.4% decrease).

Without taking clustering of metastases within patient into account, 90.4% of all nonliver metastases were ^{18}F-FES–positive and 9.6% were ^{18}F-FES–negative using the SUV_{max} threshold of 1.5. Bone, lymph node, and lung metastases were ^{18}F-FES–negative in, respectively, 8.9% (95% CI, 7.5–10.6), 8.2% (95% CI, 5.4–12.4), and 15.0% (95% CI, 8.1–26.1) (not significant; Fisher exact test P = 0.242). Patients for whom all metastases were ^{18}F-FES–positive had on average more metastases than patients with one or more ^{18}F-FES–negative metastases (23 vs. 12 metastases; independent sample t test P = 0.020). When taking these interpatient differences into account by multilevel analysis, the percentage ^{18}F-FES–positive lesions also did not differ according to metastatic site (compared with bone metastases, the difference in ^{18}F-FES positivity rate was −2.4% [95% CI, −5.6 to 0.8; P = 0.15] for lymph node

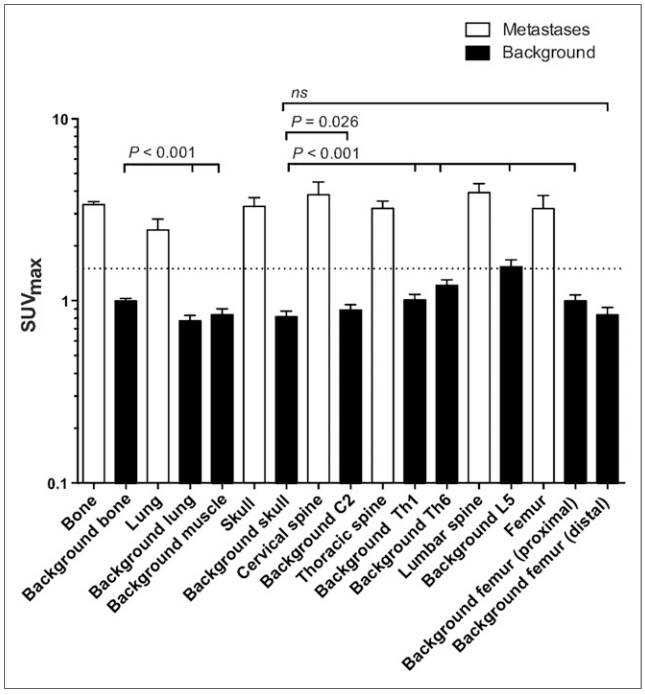

FIGURE 2. Median ^{18}F-FES uptake in healthy tissues. Geometric mean SUV_{max} was 0.99 (95% CI, 0.95–1.04) in bone, 0.77 (95% CI, 0.72–0.84) in lung, 0.64 (95% CI, 0.59–0.96) in fat, 0.84 (95% CI, 0.77–0.91) in muscle, and 15.43 (95% CI, 14.25–16.70) in liver (all P < 0.001 compared with bone). From lowest to highest background uptake, geometric mean SUV_{max} within skeleton was 0.82 (95% CI, 0.76–0.88) in skull, 0.83 (95% CI, 0.78–0.90) in distal femur, 0.89 (95% CI, 0.83–0.96) in cervical spine, 1.02 (95% CI, 0.95–1.09) in femur head, 1.02 (95% CI, 0.94–1.10) in thoracic spine Th1, 1.23 (95% CI, 1.14–1.33) in thoracic spine Th6, and 1.55 (95% CI, 1.41–1.68) in lumbar spine (all P < 0.001 compared with skull, except for cervical spine [P = 0.027] and distal femur [P = 0.62]).

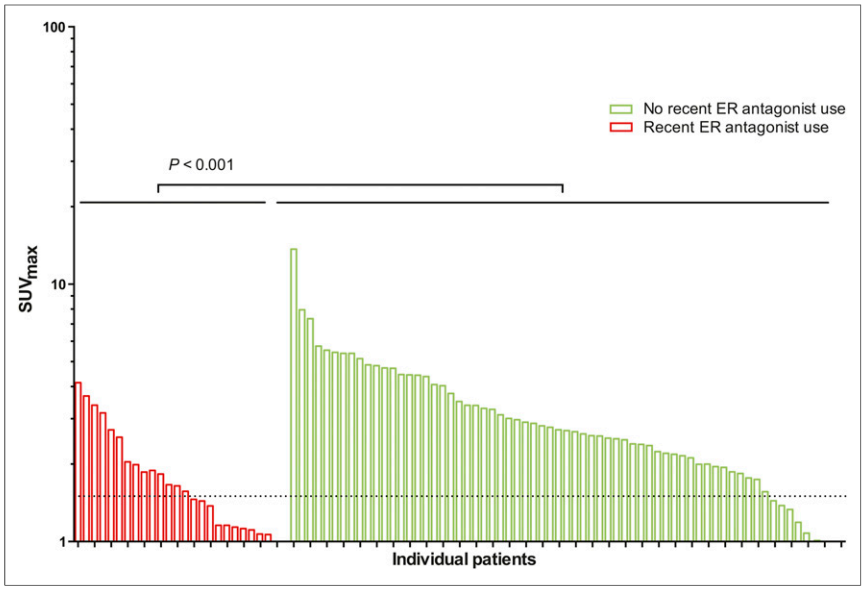

FIGURE 3. ^{18}F-FES uptake in tumor lesions per patient with and without ER antagonist use before ^{18}F-FES PET. Twenty-eight patients were withdrawn from ER antagonists (median, 5.2; range, 3–11 wk) before ^{18}F-FES PET. The geometric average of SUV_{max} was 42.1% lower (95% CI, −52.7% to −29.6%; $P < 0.001$) in patients using ER antagonists before PET than in patients who did not recently use ER antagonists.

and −3.0% (95% CI, −9.3 to 3.2; $P = 0.35$] for lung metastases). These results were also not affected by recent ER antagonist use.

Pattern of ^{18}F-FES Uptake by Normal Surrounding Tissue, per Location

Background SUV_{max} in healthy tissue differed per location (Fig. 2). Geometric mean SUV_{max} was higher in bone than in lung, fat, and muscle (all $P < 0.001$). In the skeleton, background uptake also differed per location. Of all background measurements excluding liver measurements, a remarkable 9% were higher than the SUV threshold of 1.5, namely in fat, muscle, femur, femur head, thoracic spine, and lumbar spine. In the lumbar spine, 54% of the background measurements exceeded the SUV_{max} of 1.5. In lung, skull, and cervical spine, no background measurements reached the prior set threshold of 1.5.

Effect of ER Antagonists on ^{18}F-FES Uptake in Metastases

The geometric average of SUV_{max} of metastases was 42.1% lower (95% CI, −26.6 to 52.7; $P < 0.001$) in patients who did versus those who did not recently use ER antagonists before ^{18}F-FES PET, even after a median of 5.2 wk since end of ER antagonist use (Fig. 3). After adjustment for metastatic site, this association between ER antagonist use and SUV_{max} did not change. Also, the percentage of ^{18}F-FES–negative lesions was higher in patients who only recently stopped ER antagonist use, with an absolute difference of 25.3% (95% CI, 16.3%–34.1%; $P < 0.001$). Again, adjustment for metastatic site did not affect these results. There was no difference seen in the effect of ER antagonist use for the different organs (bone, lung, lymph node, and other). No relation was observed between the duration of withdrawing from the ER antagonist and ^{18}F-FES PET and ^{18}F-FES uptake.

There was no difference in ^{18}F-FES uptake in normal tissue between patients who did versus those who did not recently use ER antagonists before ^{18}F-FES PET (4.7% lower after ER antagonist use; 95% CI, −8.3% to 16.1%; $P = 0.47$). This result was independent of the anatomic site of the background tissue.

DISCUSSION

In this study, we show heterogeneity in ^{18}F-FES uptake between tumor lesions within and between metastatic breast cancer patients with ER-positive tumors. Moreover, we show differences in ^{18}F-FES uptake between healthy tissues. Additionally, we identified 3 subgroups of patients characterized by particular metastatic sites and ^{18}F-FES PET/CT features.

To our knowledge, we are the first to evaluate on a large scale the use of simultaneous PET/CT with the ^{18}F-FES tracer. We detected diversity between ^{18}F-FES uptake in tumors within as well as between patients, underlining the heterogeneous character of breast cancer metastases in ER expression. Moreover, this approach better identifies ^{18}F-FES–negative lesions. For clinical purposes, the main advantage of the ^{18}F-FES PET/CT technique is that both molecular as well as anatomic information can be acquired simultaneously within 1 procedure. Heterogeneity in ^{18}F-FES tumor uptake has also been evaluated in a retrospective study in 91 patients who had undergone ^{18}F-FDG PET within 30 d of ^{18}F-FES PET (*17*). This study, in which 505 lesions were identified in 91 patients, showed the development of ^{18}F-FES–negative disease in 37% of patients with a previous ER-positive biopsy result. In addition, it detected only few patients who had highly discordant ^{18}F-FES uptake across tumor sites.

Although all patients included in our study had biopsy-proven ER-positive disease (primary or metastatic), 48% of the patients had one or more ^{18}F-FES–negative lesions. Moreover, 36% of the patients had both ^{18}F-FES–positive and ^{18}F-FES–negative lesions, indicating heterogeneous disease. Previous studies have shown that ^{18}F-FES– negative lesions are predictive for the absence of response to endocrine therapy (*18*).

Although the existence of tumor heterogeneity is evident, there is an ongoing debate on how to characterize this heterogeneity further and how to personalize clinical trials for optimizing treatment (*19*). Most studies focus on heterogeneity by gene expression analysis and transcriptomics, mainly on primary tumor material. With agglomerative cluster analysis on functional parameters as input variables including ^{18}F-FES uptake and metastatic site, we identified 3 distinct patterns. These clusters were mainly characterized by differences in number of metastases, metastatic site, and ^{18}F-FES uptake. Thus, in the apparent heterogeneous group of ER-positive breast cancer, several characteristics are shared by multiple patients that might indicate communal tumor evolutionary aspects. Similar to the predictive capacity of gene expression analysis for primary breast cancer, the identified imaging clusters for ^{18}F-FES PET/CT may aid in predicting treatment response in the metastatic setting.

Heterogeneity in ^{18}F-FES uptake could partly be explained by differences in organ characteristics, because bone metastases had higher ^{18}F-FES uptake than nodal and pulmonary metastases. An

earlier study, which evaluated ER expression in primary tumor and metastases by a radioactive binding assay on cytosol, described no difference between metastatic sites regarding ER expression (*20*). However, lung, bone, and liver metastases were not included in this analysis and ER expression was quantified differently from the current golden immunohistochemical standard and was scored dichotomously. In our study, interestingly, not only did bone metastases have higher ^{18}F-FES uptake, but also healthy bone had higher uptake than healthy lung and fat tissue. Bone shows estrogen responsiveness, mediated via ERα. For example, estrogen-mediated activation of ERα in osteoblasts attenuates bone resorption (*21*). ER-positive metastatic breast cancer is predominantly characterized as bone disease (*22*). Also, in our study in patients with immunohistochemically proven ER-positive breast cancer, most metastases were present in bone (78%). Together, these observations are in line with relatively high background estrogen signaling in normal bone compared with other tissues. This could possibly attract ER-positive luminal breast cancer cells to the skeleton. Colonization of cancer cells has an organ-specific character, which demands distinct cancer cells as well as host organ properties (*23*). Several microenvironmental factors, capable of modulating ER expression and signaling activity, are known to be differentially expressed among various organs (*24,25*).

In addition, other techniques can contribute to a better understanding of tumor heterogeneity such as synchronous biopsies of primary and metastatic lesions as well as autopsies (*26,27*). In this study, we show lower ^{18}F-FES uptake in lymph node and pulmonary metastases than bone metastases. This might imply that patients with bone metastases show better response to hormonal therapy than patients with pulmonary and or lymph node metastases. Evaluating heterogeneity by ^{18}F-FES PET might aid in selecting patients who respond on endocrine therapy (*28*).

In agreement with European Association of Nuclear Medicine guidelines (*14*), we used an SUV_{max} as the outcome parameter. Large lesions, however, tend to have higher SUV_{max} than small lesions, as statistically more voxels can be affected by extreme noise that leads to the hottest voxel (*29*). We have used a threshold of 1.5 or greater for the identification of ^{18}F-FES–positive lesions. Others have used an SUV_{max} cutoff of 2.0 (*30*). However, direct evidence for either of these thresholds is lacking (*10*). In our study, the 1.5 threshold was exceeded by background ^{18}F-FES uptake in various normal tissues. This could implicate the use of background-corrected SUV_{max} instead of absolute SUV_{max}. Others have suggested the use of a database-based correction, based on the average SUV_{max} of different organs (bone, lung, lymph nodes) in the setting of androgen receptor imaging with 16β-^{18}F-fluoro-5α-dihydrotestosterone PET (*31*). Our results, however, indicate that a correction on an individual basis, and per organ, is likely preferable, because the background uptake can vary between patients and locations within the same patient. Moreover, background correction would provide a more realistic quantification of the response rate in serial ^{18}F-FES PET scanning before and after intervention with antihormonal therapy as the SUV threshold is not included in the calculation. For this purpose, background subtraction has been used in a recent published study (*32*).

Finally, we were able to assess in a larger group the effects of recent ER antagonist use on ^{18}F-FES uptake. Currently, the optimal time of withdrawal of ER antagonists before PET scanning that is necessary to diminish the influence of these drugs on ^{18}F-FES uptake is unknown. For patients who stopped 3- to 12-wk use of ER antagonists before ^{18}F-FES PET, we show 42.1% lower ^{18}F-FES uptake than in patients not using these drugs before scanning. We were not able to show a relation between the time of withdrawal and ^{18}F-FES uptake. On the basis of these data, we can conclude that ER antagonists, even after the currently used withdrawal time of 5 wk in study protocols, still can considerably influence ^{18}F-FES uptake. This could be caused by competition for ER, downregulation of ER, or selection for ER-negative clones in patients treated with ER antagonists.

Our study has limitations. We retrospectively reanalyzed existing ^{18}F-FES PET scans. Metastases were identified on low-dose CT scans if no contrast-enhanced CT scan was available, which could have led to an underestimation of the total number of metastases. We have applied a 10-mm threshold for lesions detected on CT scans to rule out that ^{18}F-FES uptake in tumor lesions was only negative due to its lower resolution than the CT scan. This could have underestimated the number of ^{18}F-FES–negative lesions. However, if lesions smaller than 10 mm would have been included, false-negative ^{18}F-FES PET findings are more likely to occur and an unreliably high number of ^{18}F-FES–negative lesions would have been found. CT and ^{18}F-FES PET scans show high specificity for detection of (bone) metastases, and therefore the incidence of false-positive lesions is probably low (*12,33*).

CONCLUSION

^{18}F-FES uptake is heterogeneous between tumor lesions in metastatic breast cancer patients with ER-positive tumors and is influenced by anatomic site. Moreover, differences in ^{18}F-FES uptake are seen between healthy tissues. Additionally, we identified 3 subgroups of patients characterized by particular metastatic sites and ^{18}F-FES PET/CT features. This study improves the insights in differences between and within patients with ER-positive tumors and can eventually support intervention strategies that can adequately address this heterogeneity.

ACKNOWLEDGMENTS

This study was supported by Dutch Cancer Society grant RUG 2010-4739, ERC advanced grant 293445 (OnQview), and Alpe d'HuZes grant RUG 2012-5565 (IMPACT).

REFERENCES

1. Ferlay J, Soerjmataram I, Ervik M, et al. GLOBOCAN 2012 v1.0, cancer incidence and mortality worldwide: IARC CancerBase no. 11. International Agency for Research on Cancer website. http://globocan.iarc.fr. 2013. Accessed June 21, 2018.
2. McGranahan N, Swanton C. Clonal heterogeneity and tumor evolution: past, present, and the future. *Cell.* 2017;168:613–628.
3. Burrell RA, Swanton C. Tumour heterogeneity and the evolution of polyclonal drug resistance. *Mol Oncol.* 2014;8:1095–1111.
4. Zardavas D, Irrthum A, Swanton C, Piccart M. Clinical management of breast cancer heterogeneity. *Nat Rev Clin Oncol.* 2015;12:381–394.
5. Palmieri C, Patten DK, Januszewski A, Zucchini G, Howell SJ. Breast cancer: current and future endocrine therapies. *Mol Cell Endocrinol.* 2014;382:695–723.
6. Anderson WF, Katki HA, Rosenberg PS. Incidence of breast cancer in the United States: current and future trends. *J Natl Cancer Inst.* 2011;103:1397–1402.
7. Aurilio G, Disalvatore D, Pruneri G, et al. A meta-analysis of oestrogen receptor, progresterone receptor and human epidermal growth factor receptor 2 discordance between primary breast cancer and metastases. *Eur J Cancer.* 2014;50:277–289.
8. Amir E, Miller N, Geddie W, et al. Prospective study evaluating the impact of tissue confirmation of metastatic disease in patients with breast cancer. *J Clin Oncol.* 2012;30:587–592.
9. Peterson LM, Mankoff DA, Lawton T, et al. Quantitative imaging of estrogen receptor expression in breast cancer with PET and ^{18}F-fluoroestradiol. *J Nucl Med.* 2008;49:367–374.
10. van Kruchten M, de Vries EG, Brown M, et al. PET imaging of oestrogen receptors in patients with breast cancer. *Lancet Oncol.* 2013;14:e465–e475.

11. van Kruchten M, Glaudemans AW, de Vries EF, et al. Positron emission tomography of tumour [18F]fluoroestradiol uptake in patients with acquired hormone-resistant metastatic breast cancer prior to oestradiol therapy. *Eur J Nucl Med Mol Imaging*. 2015;42:1674–1681.
12. van Kruchten M, Glaudemans AW, de Vries EF, et al. PET imaging of estrogen receptors as a diagnostic tool for breast cancer patients presenting with a clinical dilemma. *J Nucl Med.* 2012;53:182–190.
13. Venema CM, Apollonio G, Hospers GA, et al. Recommendations and technical aspects of 16α-[^{18}F]fluoro-17β-estradiol PET to image the estrogen receptor in vivo: the Groningen experience. *Clin Nucl Med.* 2016;41:844–851.
14. Boellaard R, Delgado-Bolton R, Oyen WJ, et al. FDG PET/CT: EANM procedure guidelines for tumour imaging: version 2.0. *Eur J Nucl Med Mol Imaging*. 2015;42:328–354.
15. Sundararajan L, Linden HM, Link JM, et al. ^{18}F-fluoroestradiol. *Semin Nucl Med.* 2007;37:470–476.
16. Charrad M, Ghazzali N, Boiteau V, et al. An R package for determining the relevant number of clusters in a data set. *J Sta Soft.* 2014;61:1–36.
17. Kurland BF, Peterson LM, Lee JH, et al. Between-patient and within-patient (site-to-site) variability in estrogen receptor binding, measured in vivo by ^{18}F-fluoroestradiol PET. *J Nucl Med.* 2011;52:1541–1549.
18. Linden HM, Stekhova SA, Link JM, et al. Quantitative fluoroestradiol positron emission tomography imaging predicts response to endocrine treatment in breast cancer. *J Clin Oncol.* 2006;24:2793–2799.
19. Alizadeh AA, Aranda V, Bardelli A, et al. Toward understanding and exploiting tumor heterogeneity. *Nat Med.* 2015;21:846–853.
20. Allegra JC, Lippman ME, Thompson EB, et al. Distribution, frequency, and quantitative analysis of estrogen, progesterone, androgen, and glucocorticoid receptors in human breast cancer. *Cancer Res*. 1979;39:1447–1454.
21. Manolagas SC, O'Brien CA, Almeida M. The role of estrogen and androgen receptors in bone health and disease. *Nat Rev Endocrinol.* 2013;9:699–712.
22. Kennecke H, Yerashalmi R, Woods R, et al. Metastatic behavior of breast cancer subtypes. *J Clin Oncol.* 2010;28:3271–3277.
23. Nguyen DX, Bos PD, Massagué J. Metastasis: from dissemination to organ-specific colonization. *Nat Rev Cancer.* 2009;9:274–284.
24. Guise TA. Breast cancer bone metastases: it's all about the neighborhood. *Cell.* 2013;154:957–959.
25. Sauvé K, Lepage J, Sanchez M, et al. Positive feedback activation of estrogen receptors by the CXCL12-CXCR4 pathway. *Cancer Res.* 2009;69:5793–5800.
26. Ng CKY, Bidard FC, Piscuoglio S, et al. Genetic heterogeneity in therapy-naïve synchronous primary breast cancers and their metastases. *Clin Cancer Res.* 2017;23:4402–4415.
27. Juric D, Castel P, Griffith M, et al. Convergent loss of PTEN leads to clinical resistance to a PI(3)Kα inhibitor. *Nature.* 2015;518:240–244.
28. Kurland BF, Peterson LM, Lee JH, et al. Estrogen receptor binding (^{18}F-FES PET) and glycolytic activity (^{18}F-FDG PET) predict progression-free survival on endocrine therapy in patients with ER+ breast cancer. *Clin Cancer Res.* 2017;23:407–415.
29. Lodge MA, Chaudhry MA, Wahl RL. Noise considerations for PET quantification using maximum and peak standardized uptake value. *J Nucl Med.* 2012;53:1041–1047.
30. Dehdashti F, Mortimer JE, Trinkaus K, et al. PET-based estradiol challenge as a predictive biomarker of response to endocrine therapy in women with estrogen-receptor-positive breast cancer. *Breast Cancer Res Treat.* 2009;113:509–517.
31. Fox JJ, Autran-Blanc E, Morris MJ, et al. Practical approach for comparative analysis of multilesion molecular imaging using a semiautomated program for PET/CT. *J Nucl Med.* 2011;52:1727–1732.
32. Wang Y, Ayres KL, Goldman DA, et al. ^{18}F-fluoroestradiol PET/CT measurement of estrogen receptor suppression during a phase I trial of the novel estrogen receptor-targeted therapeutic GDC-0810: using an imaging biomarker to guide drug dosage in subsequent trials. *Clin Cancer Res.* 2017;23:3053–3060.
33. Mahner S, Schirrmacher S, Brenner W, et al. Comparison between positron emission tomography using 2-[fluorine-18]fluoro-2-deoxy-D-glucose, conventional imaging and computed tomography for staging of breast cancer. *Ann Oncol.* 2008;19:1249–1254.